

Clinical Significance of DXA and HR-pQCT in Autosomal Dominant Osteopetrosis (ADO II)

Sebastian Butscheidt¹ · Tim Rolvien¹ · Uwe Kornak^{2,3,4} · Felix N. Schmidt¹ · Thorsten Schinke¹ · Michael Amling¹ · Ralf Oheim¹

Received: 24 July 2017 / Accepted: 21 September 2017 / Published online: 10 October 2017
© Springer Science+Business Media, LLC 2017

Abstract The main hallmark of high bone mass (HBM) disorders is increased bone mineral density, potentially visible in conventional radiographs and quantifiable by other radiographic methods. While one of the most common forms of HBM is *CLCN7*-related autosomal dominant osteopetrosis type II (ADO II), there is no consensus on diagnostic thresholds. We therefore wanted to assess whether *CLCN7*-osteopetrosis patients differ from benign HBM cases in terms of (1) bone mineral density, (2) bone structure, and (3) microarchitectural abnormalities. 16 patients meeting the criteria of HBM (DXA *T/Z*-score ≥ 2.5 at all sites) were included in this retrospective study. Osteologic assessment using dual-energy X-ray absorptiometry (DXA), high-resolution peripheral quantitative computed tomography (HR-pQCT), and serum analyses was performed. The presence of *CLCN7* and/or

other HBM gene mutations affecting bone mass were tested using a custom designed bone panel. While a DXA threshold for ADO II could be implemented (DXA Z-score $\geq + 6.0$), the differences in bone microarchitecture were of lesser extent compared to the benign HBM group. All adult patients with ADO II suffered from elevated fracture rates independent from Z-score. In HR-pQCT, structural alterations, such as bone islets were found only inconsistently. In cases of HBM, a DXA Z-score ≥ 6 may be indicative for an inheritable HBM disorder, such as ADO II. Microarchitectural bone alterations might represent local microfracture repair or accumulation of cartilage remnants due to impaired osteoclast function, but seem not to be correlated with fracture risk.

Keywords High bone mass · Osteopetrosis · DXA · HR-pQCT · Bone microarchitecture · Bone islets

Electronic supplementary material The online version of this article (doi:[10.1007/s00223-017-0332-x](https://doi.org/10.1007/s00223-017-0332-x)) contains supplementary material, which is available to authorized users.

Sebastian Butscheidt and Tim Rolvien have contributed equally to this manuscript.

✉ Michael Amling
amling@uke.de

¹ Department of Osteology and Biomechanics, University Medical Center Hamburg-Eppendorf, Lottestr. 59, 22529 Hamburg, Germany

² Institute of Medical Genetics and Human Genetics, Charité Universitätsmedizin Berlin, Augustenburger Platz 1, 13353 Berlin, Germany

³ Berlin-Brandenburg Center for Regenerative Therapies, Charité Universitätsmedizin Berlin, Berlin, Germany

⁴ Max Planck Institute for Molecular Genetics, Berlin, Germany

Introduction

Roughly 99% of young adults have a bone mineral density (BMD) in the normal range, which is defined as ± 2.5 standard deviation (SD) above or below the average peak bone mass. Most attention is paid to the -2.5 SD threshold, which is crossed by a part of the population with increasing age and serves as a definition for osteoporosis according to the World Health Organization (WHO). Less information is available on the upper threshold separating benign from pathological high bone mass (HBM) conditions. In previous studies, HBM has been defined as a BMD Z-score $\geq + 2.5$ usually measured by dual-energy X-ray absorptiometry (DXA). However, no official definition for benign or pathological HBM is available neither from the

International Society For Clinical Densitometry (ISCD) nor from the WHO [1, 2].

Extreme deviations of DXA Z-score are often a sign of rare hereditary diseases. However, it has to be considered that several structural alterations of the bone such as fractures [3], osteoarthritis [4], or myelofibrosis [5] may lead to false-high BMD values. Interpreting these results, one should also differentiate between focal and generalized increases in bone mass [6]. Therefore, it is necessary to measure lumbar spine, as well as total femur [6]. The differential diagnosis of a genuine increase in bone mass ranges from tumors or renal osteodystrophy, to heritable skeletal dysplasias, among them osteopoikilosis [7], progressive diaphyseal dysplasia/Camurati-Engelmann syndrome [8], and osteopetrosis [9, 10]. The latter is a common cause of pathological high bone mass. Mutations in the *CLCN7* gene lead to the autosomal dominant osteopetrosis type II (ADO II), which is characterized by a juvenile onset and a highly variable clinical course [11, 12]. The *CLCN7* gene, which is located on chromosome 16p13, encodes the CLC-7 chloride channel [11, 13]. This anion channel takes part in the acidification of the resorption lacunae via the osteoclast's ruffled border membrane [14]. Mutations result in dysfunctional osteoclasts, leading to decreased resorption of mineralized cartilage and bone, and subsequent high bone mass in affected individuals. Often, ADO II is diagnosed accidentally on routine radiographic investigations. The most common clinical manifestation are fractures of the appendicular skeleton [10]. Less common symptoms are osteomyelitis, visual loss, hepatosplenomegaly, and bone marrow failure [10].

It is important to differentiate osteopetrosis from benign HBM, which is not associated with increased fracture risk, and from other disorders, which may indicate different specific treatment options. Gregson and colleagues provided an algorithm for the clinical management of patients with increased DXA-derived BMD values [6]. This algorithm considers the increase's distribution (focalized vs. generalized) and clinical findings such as medical and family history, blood tests, radiographs, and other imaging to elucidate the underlying cause [6]. As a final procedure, the authors ultimately suggest genetic analysis in order to rule out or to diagnose genetic disorders. However, it is not clear which increase in BMD is a clear sign for ADO II.

A recent case report examined the microarchitecture in two ADO II patients by performing high-resolution peripheral quantitative computed tomography (HR-pQCT) [15]. In addition to increases in bone structural parameters, islets of dense bone were identified resulting in a great heterogeneity within bone microarchitecture. It was hypothesized that this might contribute to the known

elevated fracture rates. However, the significance of these findings is not clear due to the low number of participants.

We performed this study in order to find out whether there is a threshold in DXA scans which makes an underlying monogenetic bone disorder, such as ADO II, very likely compared to benign HBM. Furthermore, we examined if dense bone islets are present in all ADO II patients and if they are associated with fractures. Additionally, we determined which parameters of bone microarchitecture correlate with the increased BMD in ADO II and if they are helpful in identifying ADO II patients.

Methods

Participants and Study Design

Our medical database was searched retrospectively for cases meeting the inclusion criterion of a DXA Z-score ≥ 2.5 at all sites in the years 2014–2017 and subsequent genetic analysis. A total of 16 individuals (3 male, 13 female, age range 7–79 years) with a high bone mass phenotype could be identified. All patients were referred to our specialized osteologic outpatient clinic in order to examine the high bone mass phenotype further, which was initially suspected from skeletal anomalies in plain radiographs and CT scans or pathologic fractures. Sex, age, height, and medical history were recorded. Regarding their medical history, we paid special attention to known symptoms of osteopetrosis like fractures, musculoskeletal pain, and neurologic symptoms. In order to characterize the inheritance mechanism, pedigrees were drawn for related patients. Based on the genetic analysis, two groups were established and compared to another. The *CLCN7* mutated cases ($n = 8$) included one family with three affected individuals (family A: cases A.1, A.4, A.5), one affected woman (B.1), one other family with three individuals (family C: cases C.1, C.2, C.3), and one adolescent (D.1). The other eight patients (H.1–H.8) did not show any genetic variants associated with a high bone mass phenotype and were therefore classified as benign HBM cases. The unaffected individuals of family A (cases A.2. and A.3, normal BMD) were tested negatively for *CLCN7* and served for a clinical comparison to the affected family members. However, they were not included in the HBM group.

All examinations were performed for clinical indications; yet informed consent was obtained from all patients. The presented data was analyzed in a retrospective study design.

Genetic Analysis

All 25 exons of the *CLCN7* gene (chromosome 16p13) were amplified by PCR including flanking intronic sequences and subsequently sequenced by the Sanger method. In cases of absence of a *CLCN7* mutation, all known genes leading to skeletal dysplasias with high bone mass including *SOST*, *TCIRG1*, *TGFB1*, *OSTM1*, *SNX10*, *TNFSF11*, *TNFRSF11A*, *ANKH*, *LEMD3*, *FAM20C*, *LRP5*, and *CTSK* were tested by next generation sequencing (NGS) using a custom designed bone mass gene panel (Sure Select, Agilent). Sequencing was performed on a MiSeq machine (Illumina, San Diego, CA, USA). Bioinformatic analysis comprised variant calling using ANNOVAR and variant filtering and interpretation by GeneTalk and PhenIX [16, 17]. The pathogenicity of the prioritized variants was analyzed using MutationTaster, Polyphen, and SIFT [18–20].

Skeletal Status

In order to characterize bone turnover, blood samples were drawn from every participant and biochemical analysis was performed of the following parameters: calcium (Ca), phosphate (P), osteocalcin (OC), 25-hydroxyvitamin D (25-OH-D₃), bone alkaline phosphatase (BAP), parathyroid hormone (PTH), deoxypyridinoline (DPD), creatinine kinase (CK), and fibroblast growth factor 23 (FGF-23).

Areal bone mineral density (aBMD) was assessed in all cases by performing dual-energy X-ray absorptiometry (DXA; Lunar iDXA; GE Healthcare; Madison, WI, USA) of the lumbar spine and both femoral necks. In Cases A.1 and B.1 aBMD was evaluated at lumbar spine only because osteosynthesis due to pathological femoral fractures had been performed. Results are given as aBMD (absolute values, g/cm²) and Z-score in order to enable comparisons between the cases as four children were enrolled in the study.

Radiographs of the lumbar spine, hand, and pelvis were taken of cases A.1, A.4, A.5, and additionally of the lumbar spine and hand of the healthy family members A.2 and A.3.

For further analysis of the skeletal status, seven *CLCN7* patients and eight benign HBM cases underwent high-resolution peripheral quantitative computed tomography (HR-pQCT; XtremeCT, Scanco Medical, Brüttisellen, Switzerland) in order to evaluate bone microarchitecture. Therefore, scans of the non-dominant distal radius and distal tibia were performed. In case of a previous fracture on the desired site, the opposite extremity was scanned. Scout views were used to set reference lines at the junction of the medial and distal thirds of the distal radius and at the level of the tibial plafond as described previously [21]. In children growth plates were excluded as suggested by

Burrows and colleagues [22]. Results were compared to the 50th centile of site-, age-, and sex-specific reference values [23]. The differences were calculated and presented graphically in %. Furthermore, three-dimensional reconstructions of the scanned area were calculated for each *CLCN7* case and examined with regard to anomalies of bone microarchitecture. Representative 2D images were saved and presented for every *CLCN7* case.

To verify the histologic characteristics of *CLCN7* related osteopetrosis, a diagnostic iliac crest bone biopsy was obtained from case C.1 following the protocol by Bordier and colleagues [24]. The extracted material was fixed in 3.7% formaldehyde, dehydrated in ascending concentrations of ethanol, and embedded in methyl methacrylate. Undecalcified sections were cut on a Microtec rotation microtome (CVT 4060E; Micro Tec, Walldorf, Germany) with a thickness of 5 µm and routinely stained with toluidine blue, trichrome Masson-Goldner, von Kossa/van Gieson. Histomorphometric evaluation was carried out using Osteomeasure histomorphometry software (Osteometrics, Atlanta, GA, USA). The performed analysis and nomenclature of histomorphometric parameters conform with the ASBMR standards [25]. Results were compared with sex- and age-specific reference values from the literature [26] as well as 5 sex- and age-specific controls from our database (mean age 42.2 ± 3.2).

Measurement of bone mineral density distribution (BMDD) was performed by quantitative backscattered electron imaging (qBEI; LEO 435 VP; LEO Electron Microscopy Ltd., Cambridge, England, UK) as described previously [27]. Four images were taken (magnification 100x) and analyzed using Image J (v.1.42, National Institutes of Health, Bethesda, MD, USA). Ca mean was determined by transformation of the greyscale values as described by our group [27]. Results were compared to a sex- and age-specific control of our database.

Statistical Analysis

Results are given as absolute values or mean ± SD if appropriate. Significance of the presented data was analyzed using the two-tailed Student's *t* test for unpaired data (Excel for Mac 2011, Microsoft, v.14.0.0). Level of significance is defined as $p < 0.05$. Additionally, Receiver Operating Characteristic (ROC) curve analysis was performed to find the optimal DXA Z-score threshold with the highest sensitivity but lowest false-positive rate.

Results

Basic Genetic and Skeletal Characterization

In eight patients from four families, genetic analysis revealed mutations in the *CLCN7* gene (c.857G > A (p.Arg286Glu), c.1773G > TA (p.Lys591Asn), c.2272T > C (p.Phe758Leu), and c.296A > G (p.Tyr99-Tys)) consistent with the diagnosis ADO II (Fig. 1a–c). While p.Arg286Glu [28], p.Phe758Leu [29], and p.Tyr99Tys [30] have been reported previously, p.Lys591Asn has not been described before; however, it was ranked to be highly pathogenic. Six of these cases had one or more fractures in their medical history. Only two young children, 8 and 9 years of age respectively, did not suffer from any fractures so far. Additionally, Case A.1 suffered from rheumatoid arthritis and recurrent inflammation of the jawbone, while case B.1 had also been previously diagnosed with rheumatoid arthritis. Case D.1 presented with 15 fractures, osteomyelitis, bone pain, and slipped capital femoral epiphysis (SCFE). For clinical and fracture history see Fig. 1a.

Within the benign HBM group, only two individuals had suffered from traumatic fractures (one scaphoid and one vertebral body fracture). None of the cases were taking any medication or had any diseases with relevance to bone mass or metabolism (i.e., steroids).

Laboratory results for bone turnover showed increased DPD levels (Fig. 1d) in cases A.1 and B.1. CK and FGF-23 levels were available for cases C.1, C.3, and D.1 only. CK activity was increased in those patients, while FGF-23 appeared within the reference range (Fig. 1d).

Radiographs were taken for affected individuals from family A (cases A1, A4, A5), as well as for 2 unaffected family members (A.2, A.3). The images revealed characteristic signs of ADO like “rugger jersey” spine (Fig. 2a) and a generalized increased bone density, especially visible in metacarpals (Fig. 2b) and iliac wings (Fig. 2c). The husband (A.2; M, 45 years) and a 3rd child (A.3; M, 15 years) were healthy and showed a normal skeletal appearance. Case A.1 underwent surgery due to pathological bilateral femur fractures, which is a characteristic for ADO II.

In order to histologically confirm the bone phenotype of ADO II, an iliac crest biopsy was obtained in case A.1. The analysis revealed a high bone mass and large, flat-shaped osteoclasts with increased numbers of nuclei, and characteristic cartilage remnants (Fig. 3a, b). Histomorphometry showed an increase in bone volume (BV/TV), trabecular number (Tb.N), and trabecular thickness (Tb.Th) compared to five sex- and age-matched controls from our control collective, as well as to sex- and age-specific reference

values from the literature [26] (Fig. 3c). Trabecular separation was reduced consecutively. Osteoclast number (N.Oc/B.pm) and osteoclast surface (Oc.S/BS) were increased.

BMDD analysis revealed higher mineralized trabeculae with highly mineralized islets compared to a healthy controls (Fig. 3d) and a matching increase of BMDD parameters, additionally compared to reference data from the literature (Fig. 3e).

DXA Z-Score Threshold for ADO II

The performed DXA scans revealed increased BMD in patients with ADO II resulting in high Z-scores at the lumbar spine (L1-4, mean: 11.2 ± 3.0), total femur left (TF L, mean: 11.9 ± 2.8) and right (TF R, mean: 10.8 ± 1.7) (Fig. 4a). DXA-derived images of an ADO II patient show the characteristic sclerosis of the vertebral endplates (“rugger jersey” spine/sandwich vertebrae) and iliac wings with a possible stenosis of the intramedullary canal of the femur. A comparable image of a benign HBM patient revealed a more evenly distributed sclerosis of the vertebral bodies and the femur (Fig. 4b). The eight benign HBM cases, who did not have any mutation in the *CLCN7* gene or any other gene related to HBM like *SOST* or *LRP5* (Supplemental Table), revealed significantly lower mean Z-scores within this group for lumbar spine, total femur left and right of 4.7 ± 1.7 ($p < 0.05$), 3.5 ± 1.1 ($p < 0.001$) and 3.7 ± 1.3 , respectively ($p < 0.001$, Fig. 4c). Receiver operating characteristic (ROC) curve analysis revealed a DXA Z-score of +6.0 as an appropriate threshold in differentiating between ADO II and benign HBM cases.

Bone Islets and Their Relation to Fractures in HR-pQCT

HR-pQCT was available for seven of the eight ADO II patients. Analysis of the two-dimensional slices and reconstructed three-dimensional models revealed dense bone islets in cases B.1, C.2, and D.1 from three different families (Fig. 5a, b). All three cases had multiple fractures in the past. Comparable alterations in bone microarchitecture could neither be detected in the remaining *CLCN7* mutated adults (cases A.1 and C.1, Fig. 5a) nor in the two affected children (cases A.4, A.5, Fig. 5b). Whereas cases A.4 and A.5 did not suffer from fractures, cases A.1 and C.1 showed a minimum of one fracture in their medical history. Interestingly case C.1 (mother) did not show dense bone islets while her son (case C.2), carrying the same mutation, presented with apparent abnormalities in bone microarchitecture including bone islets. Analysis of two-dimensional HR-pQCT images of two healthy individuals (A.2 and A.3) showed a less dense trabecular pattern than

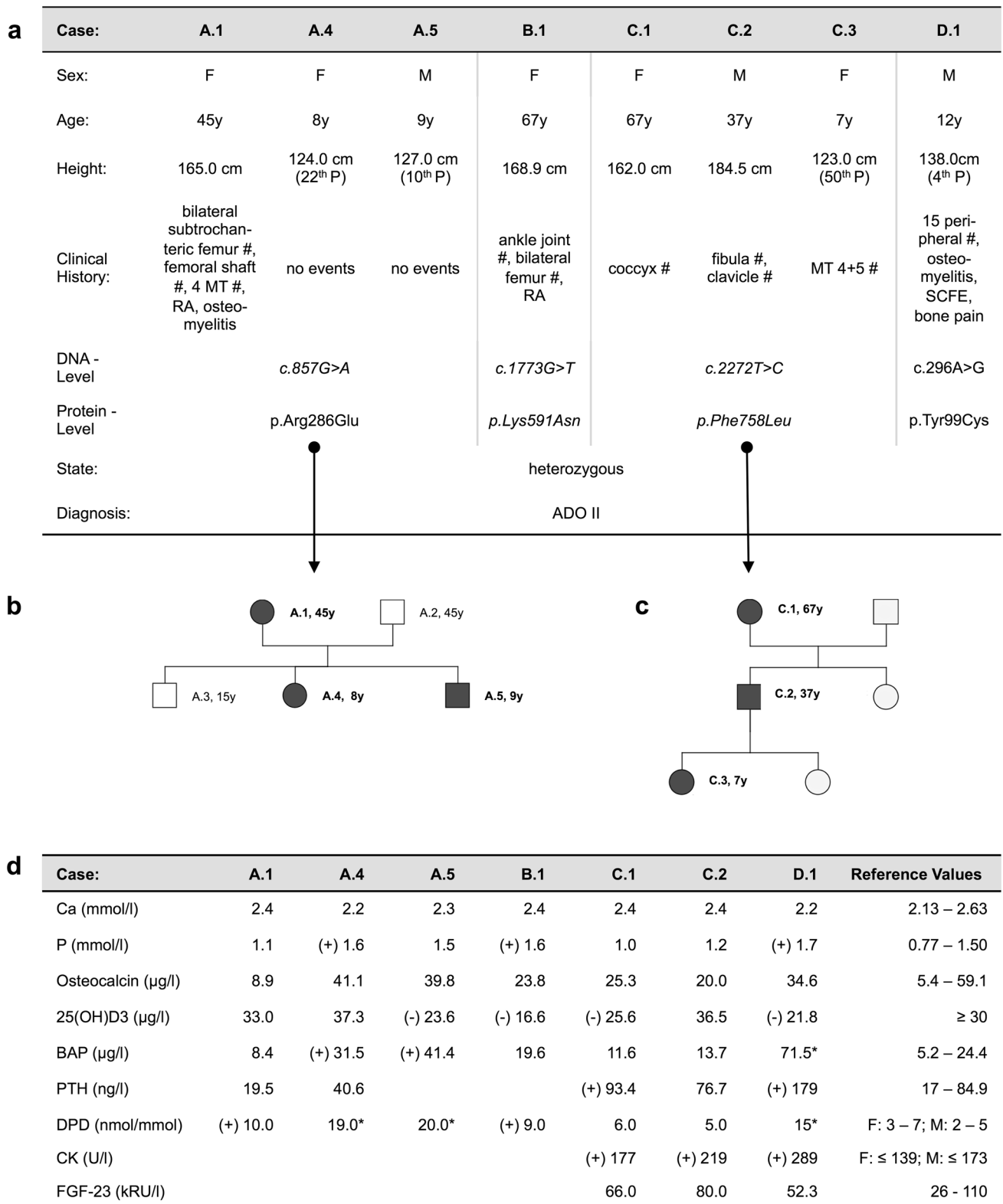


Fig. 1 Overview of eight individuals with ADO II: **a** clinical characterization; **b** pedigree of family A; **c** pedigree of family C; **d** blood test results: (+) and (-) indicating deviation from reference

values. RA rheumatoid arthritis, F female, M male, yr years, # fracture, SCFE slipped capital femoral epiphysis, MT metatarsal



Fig. 2 Radiographic examination of family A reveals characteristic signs in three family members being diagnosed with ADO II (cases A.1, A.4, A.5) but not in the two healthy controls (A.2, A.3): **a** lateral

radiograph of the lumbar spine showing a “rugged jersey” spine; **b** AP radiographs of the hand with sclerosis of phalanges; **c** AP radiographs of the pelvis with a “bone within bone” appearance of the iliac wings

the affected patients and no bone islets (images not included).

Bone Microarchitecture in ADO II and HBM Cases

Analysis of bone microarchitecture assessed by HR-pQCT of seven ADO II patients and six benign HBM cases revealed a significantly higher trabecular number (Tb.N) at the tibia for patients with ADO II ($p < 0.05$). We found a significantly higher cortical BMD (Ct.BMD) at the tibia in benign HBM compared to ADO II cases ($p < 0.05$). The other parameters did not show significant differences (Fig. 5c).

Discussion

It is well known that patients with ADO II have an overall increased BMD assessed by DXA [10, 15, 31] whereas HR-pQCT data are available for only two patients with marked elevations of structural parameters in bone microarchitecture [15]. Furthermore, it is not clear if their application provides additional information and might be beneficial in discriminating different high bone mass phenotypes. Therefore, we compared eight ADO II patients with eight benign HBM cases in order to identify significant differences in BMD and bone microarchitecture. We here provide important additional data on the bone microarchitecture in ADO II patients and suggest a BMD threshold, which may be used as a criterion for this disease.

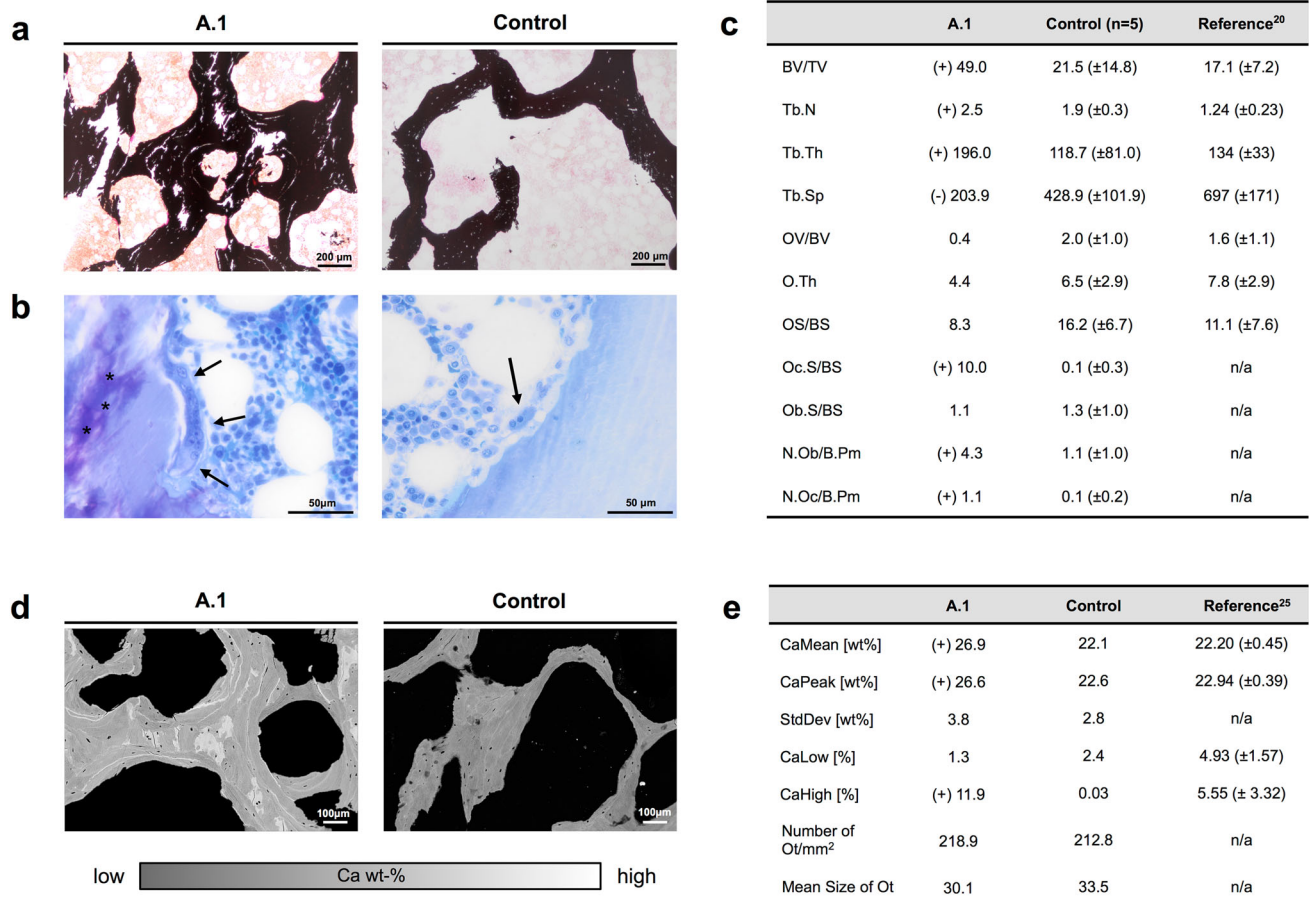


Fig. 3 Histomorphometry and BMDD analysis for case A.1 (left) and a healthy control (right): **a** sections stained by von Kossa/van Gieson demonstrating high bone mass in case A.1; **b**, toluidine blue-stained sections showing characteristic enlarged, multinuclear osteoclasts in case A.1 (black arrow), asterisks indicating cartilage remnants; **c** histomorphometry data given as mean \pm standard deviation (SD) compared to 5 healthy controls and reference data from the literature

[26], *n/a* data not available; **d** backscattered electron images revealing inhomogenously distributed, highly mineralized bone in case A.1, mean calcium content represented by bright and dark areas, indicating high and low mineralization, respectively; **e** qBEI data of an ADO II patient (case A.1) compared to a healthy control and reference data from the literature [39]; *n/a* data not available

All ADO II patients demonstrated DXA Z-scores ≥ 6.2 at all sites (Fig. 4a). Since previous studies revealed comparable results regarding DXA Z-score values [10, 15, 31], we suggest a DXA Z-score of +6.0 as a possible threshold above which the diagnosis of a clinically relevant ADO II is highly likely (Fig. 4c).

Regarding this threshold two aspects need to be further discussed. First, Waguespack et al. found that approximately 30% of *CLCN7* mutation carriers do not develop the classical signs of ADO II. These individuals had only an average DXA Z-score between +1 and +2 [10]. With the strict threshold suggested here, these individuals would not be detected. Second, next to the cohort of *CLCN7* cases analyzed in this study, other HBM mutations such as *SOST* or *LRP5* need to be considered as major differential diagnosis [32].

In benign HBM cases, the DXA Z-scores were significantly lower (Fig. 4c) and ranged from +1.8 to +8.2 at

all sites. The maximum DXA Z-score of +8.2 was detected at the lumbar spine, possibly a false-high result due to degenerative alterations of the spine. Therefore, it can be stated that DXA Z-scores of $\geq +2.5$ should be referred to as high bone mass with here initially only a low risk of a pathological condition. From a DXA Z-score $\geq +4$, the likelihood for complications and an underlying genetic cause rises significantly [6]. Above a Z-score of +6.0, which on the basis of the normal distribution of BMD can be expected in 1:1.000.000 individuals, a pathological bone condition (i.e., monogenetic) is very likely according to our data. This graduated approach may be helpful in the diagnostic algorithm, as only 3% of HBM conditions may occur due to a monogenetic disorder [32].

Beside skull and pelvis, the lumbar spine is one of the most common sides affected by osteopetrosis. Given the knowledge of characteristic signs of ADO II, such as “ruger jersey” spine or a “bone within bone” appearance,

a

| | A.1 | | A.4 | | A.5 | | B.1 | | C.1 | | C.2 | | C.3 | | D.1 | |
|-------------|-------|-----|-------|-----|-------|------|-------|------|-------|------|-------|-----|-------|------|-------|------|
| | BMD | Z | BMD | Z | BMD | Z | BMD | Z | BMD | Z | BMD | Z | BMD | Z | BMD | Z |
| L1-4 | 2.016 | 6.2 | 1.454 | 8.9 | 2.052 | 15.6 | 2.495 | 12.0 | 2.749 | 14.7 | 2.375 | 9.6 | 1.421 | 9.5 | 2.342 | 13.0 |
| TF L | * | * | 1.466 | 8.7 | 2.058 | 14.9 | * | * | 2.412 | 13.4 | 2.293 | 9.4 | 1.452 | 12.4 | * | * |
| TF R | * | * | 1.455 | 8.6 | 1.884 | 12.9 | * | * | 2.328 | 12.3 | 2.232 | 8.9 | 1.411 | 11.8 | 1.937 | 10.0 |

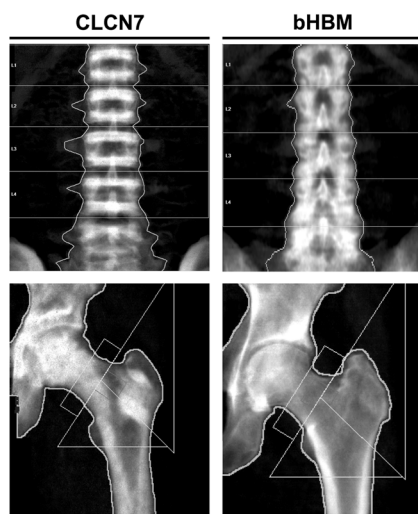
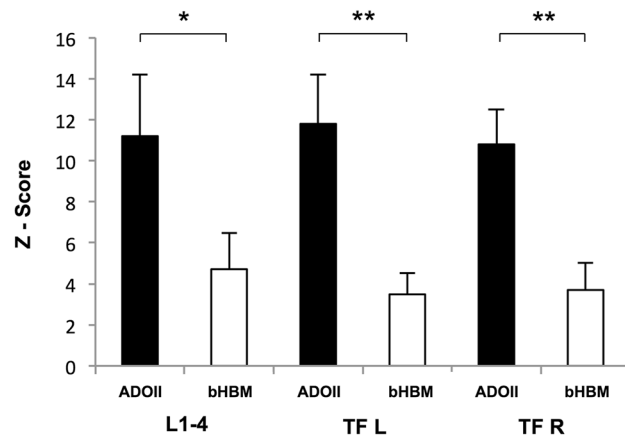
b**c**

Fig. 4 Assessment of BMD using DXA: **a** absolute BMD values and Z-score in eight ADO II cases; **b** representative DXA-derived images of lumbar spine and left femur: *CLCN7* case (left) with a characteristic “rugger jersey” spine and a “bone within bone” appearance of femur and pelvis; benign HBM (bHBM) case (right)

DXA-derived images may provide additional diagnostic information in order to identify individuals with ADO II among patients with elevated Z-Scores (Fig. 4b). Compared to common radiographs or computed tomography, these tools also require a smaller radiation dose and should therefore be considered a higher priority in the diagnostic algorithm, especially if children are involved. Additionally, analysis of creatine kinase (CK) in three cases revealed elevated serum levels (Fig. 1d). This elevation is characteristic for osteopetrosis patients in general and is caused by the brain isoenzyme BB-CK [33].

Arruda and colleagues hypothesized that dense bone islets, which they observed in two ADO II patients by HR-pQCT, may contribute to the known high fracture rates in these patients [15]. The HR-pQCT analysis of seven ADO II patients in this study revealed that these islets were

presenting with a more evenly distributed increase in bone density; **c** comparison of mean Z-scores in eight ADO II patients and eight benign HBM cases; asterisks indicating significant differences; *L1-4* lumbar spine, *TF L* total femur left and *TF R* total femur right

present in only three cases, however, fractures had been observed in all examined patients, except the children (cases A.4 and A.5). Regarding this, it has to be taken into account that the clinical manifestation of this disease becomes more apparent over time so that adults have a higher risk to sustain fractures [10]. Even for the same mutation within one family (Fig. 1c), we could not find a consistent appearance of bone islets. While case C.2 showed a significant heterogeneity, his mother (case C.1) did not reveal any similar alterations. Based on our data, the dense bone islets seem to have a higher prevalence in patients with ADO II, but may not be obligatory. Consequently, their role in the explanation of the high fracture rates tends to be of lesser importance.

In fact, possible reasons for this appearance in HR-pQCT could be wide-ranging and may correlate with

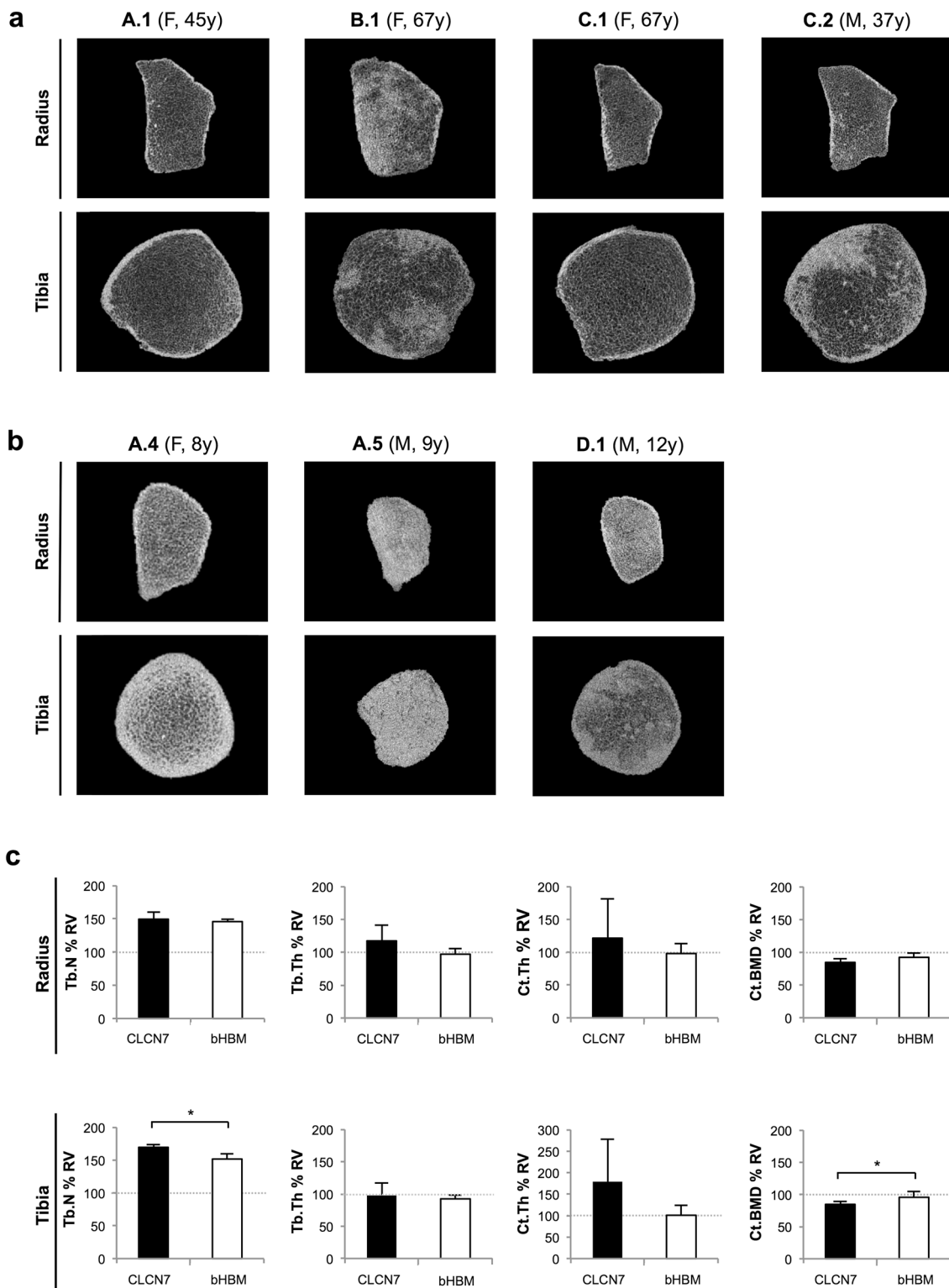


Fig. 5 Analysis of bone microarchitecture by HR-pQCT of radius and tibia: **a** reconstructed images of four adult ADO II cases with (B.1, C.2) and without (A.1, C.1) visible structural alterations; **b** reconstructed images of three children with ADO II (A.4, A.5, D.1) revealing dense bone islets only in case D.1; **c** comparison of structural parameters in seven individuals with ADO II and six benign

HBM (bHBM) cases; results given in % of the 50th centile of age-, site- and sex-specific reference values (RV) [23]; *Tb.N* trabecular number, *Tb.Th* trabecular thickness, *Ct.Th* cortical thickness, *Ct.BMD* cortical bone mineral density; asterisk indicating significant differences between *CLCN7* and benign HBM cases

typical features on the microscopic level: (1) microfractures of trabecular bone may lead to the development and consecutive accumulation of microcallus formations (MCFs) [34]; (2) impaired bone remodeling due to dysfunctional osteoclasts could lead to higher mineralized bone and brittleness resulting in an increased risk of fractures [35]; (3) dysfunctional osteoclasts may cause an impaired endochondral ossification with mineralized cartilage, which cannot be resorbed and replaced by mature bone matrix [36]. These features can be detected in histologic sections of murine [37, 38] and human biopsies (Fig. 3b, d). Regarding the latter, osteoclastic dysfunction could lead to an accumulation of cartilage remnants in certain areas, possibly resulting in dense bone islets seen in HR-pQCT images. A further clarification of such islets would require a bone biopsy in order to examine the underlying pathology.

With regard to the significant differences of the performed DXA scans between benign HBM and ADO II patients, we expected similar findings in the analysis of bone microarchitecture by HR-pQCT. Surprisingly, hardly any significant differences were discovered. Only the trabecular number (Tb.N) at the tibia, but not at the radius, was significantly increased in patients with ADO II (Fig. 5c). The observed elevation of aBMD in DXA scans might be caused by the increased trabecular number and the highly mineralized cancellous bone that was also detected by qBEI. Based on our results, the application of HR-pQCT is helpful in detecting high bone mass phenotypes, but appears to be of lesser importance in the diagnostic clarification of an existing ADO II.

As a limitation, the sample size of this study may not be statistically sufficient in order to establish a diagnostic threshold. Furthermore, the included individuals represent a highly selected cohort as some cases were referred to our outpatient clinic due to clinical and radiological features. Therefore, our data should be confirmed in a wider population including individuals solely detected by high bone mass on DXA. However, in consideration of previously published findings, our data represent a significant advance in the understanding and management of high bone mass disorders. Further studies may lead to an adjustment of the DXA threshold by providing additional data from a larger patient collective.

Taken together, our results showed marked elevations of BMD and inconsistent increases of structural parameters of bone microarchitecture in patients with ADO II. The comparison with benign HBM cases revealed significant higher DXA Z-scores in the ADO II patients leading to a threshold of + 6.0 (Z-score) at any site, which may enable clinicians to identify affected individuals by DXA measurements. As an additional consequence, we suggest a DXA Z-score of $\geq + 2.5$ as a definition for high bone

mass in consideration of an increasing likelihood for a pathological condition at DXA Z-scores $\geq + 4.0$. The application of HR-pQCT is able to detect high bone mass phenotypes but may not be beneficial in the further diagnostic distinction of the underlying diseases. High fracture risk is the most common clinical manifestation in patients with ADO II. The recently discovered dense bone islets may not be obligatory but contribute to the existing heterogeneity of bone and may therefore play a role in the development of fractures. Our data provides additional information of the high bone mass phenotype in patients with ADO II and therefore improves the clinical assessment of HBM.

Acknowledgements We thank Elke Leicht for expert technical assistance in preparing the histological sections. Furthermore, Felix Schmidt acknowledges the Joachim Herz Stiftung for a PhD Scholarship in cooperation with the PIER Helmholtz Graduate School, University of Hamburg and DESY Hamburg.

Funding This project has received funding from the European Community's Seventh Framework Programme under grant agreement no. 602300 (SYBIL) and the German Federal Ministry of Education and Research (BMBF) within the project "Detection and Individualized Management of Early Onset Osteoporosis (DIMEOS)".

Compliance with Ethical Standards

Conflict of interest Sebastian Butscheidt, Tim Rolvien, Uwe Kornak, Felix Schmidt, Thorsten Schinke, Michael Amling, and Ralf Oheim declare that they have no conflict of interest.

Human and Animal Rights All procedures performed in studies involving human participants were in accordance with the ethical standards of the institutional and/or national research committee and with the 1964 Helsinki declaration and its later amendments or comparable ethical standards.

Informed Consent Informed consent was obtained from all individual participants included in the study.

References

1. Morgan SL, Peace F, Lopez-Ben R, Fineberg N (2010) Distribution of Z-scores in a University cohort with an emphasis on "high" bone mineral density. *J Clin Densitom* 13(4):385–391. doi:10.1016/j.jocd.2010.07.003
2. Lomholt S, Amstrup AK, Moser E, Jakobsen NF, Mosekilde L, Vestergaard P, Rejnmark L (2015) Unexplained high BMD in DXA-scanned patients is generalized throughout the skeleton and characterized by thicker cortical and trabecular bone. *Calcif Tissue Int* 96(4):284–294. doi:10.1007/s00223-015-9955-y
3. Scane AC, Masud T, Johnson FJ, Francis RM (1994) The reliability of diagnosing osteoporosis from spinal radiographs. *Age Ageing* 23(4):283–286
4. Liu G, Peacock M, Eilam O, Dorulla G, Braunstein E, Johnston CC (1997) Effect of osteoarthritis in the lumbar spine and hip on bone mineral density and diagnosis of osteoporosis in elderly men and women. *Osteoporos Int* 7(6):564–569

5. Diamond T, Smith A, Schnier R, Manoharan A (2002) Syndrome of myelofibrosis and osteosclerosis: a series of case reports and review of the literature. *Bone* 30(3):498–501
6. Gregson CL, Hardcastle SA, Cooper C, Tobias JH (2013) Friend or foe: high bone mineral density on routine bone density scanning, a review of causes and management. *Rheumatology (Oxford)* 52(6):968–985. doi:10.1093/rheumatology/ket007
7. Hellemans J, Preobrazhenska O, Willaert A, Debeer P, Verdonk PC, Costa T, Janssens K, Menten B, Van Roy N, Vermeulen SJ, Savarirayan R, Van Hul W, Vanhoenacker F, Huylebroeck D, De Paepe A, Naeyaert JM, Vandesompele J, Speleman F, Verschueren K, Coucke PJ, Mortier GR (2004) Loss-of-function mutations in LEMD3 result in osteopoikilosis, Buschke-Ollendorff syndrome and melorheostosis. *Nat Genet* 36(11):1213–1218. doi:10.1038/ng1453
8. Whyte MP, Totty WG, Novack DV, Zhang X, Wenkert D, Mumm S (2011) Camurati-Engelmann disease: unique variant featuring a novel mutation in TGFbeta1 encoding transforming growth factor beta 1 and a missense change in TNFSF11 encoding RANK ligand. *J Bone Miner Res* 26(5):920–933. doi:10.1002/jbmr.283
9. Benichou O, Cleiren E, Gram J, Bollerslev J, de Vernejoul MC, Van Hul W (2001) Mapping of autosomal dominant osteopetrosis type II (Albers-Schonberg disease) to chromosome 16p13.3. *Am J Hum Genet* 69(3):647–654. doi:10.1086/323132
10. Waguespack SG, Hui SL, Dimeglio LA, Econs MJ (2007) Autosomal dominant osteopetrosis: clinical severity and natural history of 94 subjects with a chloride channel 7 gene mutation. *J Clin Endocrinol Metab* 92(3):771–778. doi:10.1210/jc.2006-1986
11. Kornak U, Kasper D, Bosl MR, Kaiser E, Schweizer M, Schulz A, Friedrich W, Delling G, Jentsch TJ (2001) Loss of the CIC-7 chloride channel leads to osteopetrosis in mice and man. *Cell* 104(2):205–215
12. Cleiren E, Benichou O, Van Hul E, Gram J, Bollerslev J, Singer FR, Beaverson K, Aledo A, Whyte MP, Yoneyama T, deVernejoul MC, Van Hul W (2001) Albers-Schonberg disease (autosomal dominant osteopetrosis, type II) results from mutations in the CLCN7 chloride channel gene. *Hum Mol Genet* 10(25):2861–2867
13. Kornak U, Schulz A, Friedrich W, Uhlhaas S, Kremens B, Voit T, Hasan C, Bode U, Jentsch TJ, Kubisch C (2000) Mutations in the a3 subunit of the vacuolar H(+)-ATPase cause infantile malignant osteopetrosis. *Hum Mol Genet* 9(13):2059–2063
14. Barvencik F, Kurth I, Koehne T, Stauber T, Zustin J, Tsiakas K, Ludwig CF, Beil FT, Pestka JM, Hahn M, Santer R, Supanchart C, Kornak U, Del Fattore A, Jentsch TJ, Teti A, Schulz A, Schinke T, Amling M (2014) CLCN7 and TCIRG1 mutations differentially affect bone matrix mineralization in osteopetrotic individuals. *J Bone Miner Res* 29(4):982–991. doi:10.1002/jbmr.2100
15. Arruda M, Coelho MC, Moraes AB, de Paula Paranhos-Neto F, Madeira M, Farias ML, Neto LV (2016) Bone mineral density and microarchitecture in patients with autosomal dominant osteopetrosis: a report of two cases. *J Bone Miner Res* 31(3):657–662. doi:10.1002/jbmr.2715
16. Kamphans T, Krawitz PM (2012) GeneTalk: an expert exchange platform for assessing rare sequence variants in personal genomes. *Bioinformatics* 28(19):2515–2516. doi:10.1093/bioinformatics/bts462
17. Zemojtel T, Kohler S, Mackenroth L, Jager M, Hecht J, Krawitz P, Graul-Neumann L, Doelken S, Ehmke N, Spielmann M, Oien NC, Schweiger MR, Kruger U, Frommer G, Fischer B, Kornak U, Flottmann R, Ardehshirdavani A, Moreau Y, Lewis SE, Haendel M, Smedley D, Horn D, Mundlos S, Robinson PN (2014) Effective diagnosis of genetic disease by computational phenotype analysis of the disease-associated genome. *Sci Transl Med* 6(252):252ra123. doi:10.1126/scitranslmed.3009262
18. Schwarz JM, Rodelsperger C, Schuelke M, Seelow D (2010) MutationTaster evaluates disease-causing potential of sequence alterations. *Nat Methods* 7(8):575–576. doi:10.1038/nmeth0810-575
19. Adzhubei IA, Schmidt S, Peshkin L, Ramensky VE, Gerasimova A, Bork P, Kondrashov AS, Sunyaev SR (2010) A method and server for predicting damaging missense mutations. *Nat Methods* 7(4):248–249. doi:10.1038/nmeth0410-248
20. Doerks T, Copley RR, Schultz J, Ponting CP, Bork P (2002) Systematic identification of novel protein domain families associated with nuclear functions. *Genome Res* 12(1):47–56. doi:10.1101/gr.203201
21. Milovanovic P, Adamu U, Simon MJ, Rolvien T, Djuric M, Amling M, Busse B (2015) Age- and sex-specific bone structure patterns portend bone fragility in radii and tibiae in relation to osteodensitometry: a high-resolution peripheral quantitative computed tomography study in 385 individuals. *J Gerontol A Biol Sci Med Sci* 70(10):1269–1275. doi:10.1093/gerona/glv052
22. Burrows M, Liu D, Perdios A, Moore S, Mulpuri K, McKay H (2010) Assessing bone microstructure at the distal radius in children and adolescents using HR-pQCT: a methodological pilot study. *J Clin Densitom* 13(4):451–455. doi:10.1016/j.jocd.2010.02.003
23. Burt LA, Liang Z, Sajobi TT, Hanley DA, Boyd SK (2016) Sex- and site-specific normative data curves for HR-pQCT. *J Bone Miner Res*. doi:10.1002/jbmr.2873
24. Bordier P, Matrajt H, Hioco D, Hepner GW, Thompson GR, Booth CC (1968) Subclinical vitamin-D deficiency following gastric surgery. Histological evidence in bone. *Lancet* 1(7540):437–440
25. Dempster DW, Compston JE, Drezner MK, Glorieux FH, Kanis JA, Malluche H, Meunier PJ, Ott SM, Recker RR, Parfitt AM (2013) Standardized nomenclature, symbols, and units for bone histomorphometry: a 2012 update of the report of the ASBMR Histomorphometry Nomenclature Committee. *J Bone Miner Res* 28(1):2–17. doi:10.1002/jbmr.1805
26. Schnitzler CM, Pettifor JM, Mesquita JM, Bird MD, Schnaid E, Smyth AE (1990) Histomorphometry of iliac crest bone in 346 normal black and white South African adults. *Bone Miner* 10(3):183–199
27. Koehne T, Vettorazzi E, Kusters N, Luneburg R, Kahl-Nieke B, Puschel K, Amling M, Busse B (2014) Trends in trabecular architecture and bone mineral density distribution in 152 individuals aged 30–90 years. *Bone* 66:31–38. doi:10.1016/j.bone.2014.05.010
28. Frattini A, Pangrazio A, Susani L, Sobacchi C, Mirolo M, Abinun M, Andolina M, Flanagan A, Horwitz EM, Mihci E, Notarangelo LD, Ramenghi U, Teti A, Van Hove J, Vujic D, Young T, Albertini A, Orchard PJ, Vezzoni P, Villa A (2003) Chloride channel CLCN7 mutations are responsible for severe recessive, dominant, and intermediate osteopetrosis. *J Bone Miner Res* 18(10):1740–1747. doi:10.1359/jbmr.2003.18.10.1740
29. Pangrazio A, Pusch M, Caldana E, Frattini A, Lanino E, Tamhankar PM, Phadke S, Lopez AG, Orchard P, Mihci E, Abinun M, Wright M, Vettenranta K, Bariae I, Melis D, Tezcan I, Baumann C, Locatelli F, Zecca M, Horwitz E, Mansour LS, Van Rooij M, Vezzoni P, Villa A, Sobacchi C (2010) Molecular and clinical heterogeneity in CLCN7-dependent osteopetrosis: report of 20 novel mutations. *Hum Mutat* 31(1):E1071–1080. doi:10.1002/humu.21167
30. Del Fattore A, Peruzzi B, Rucci N, Recchia I, Cappariello A, Longo M, Fortunati D, Ballanti P, Iacobini M, Luciani M, Devito R, Pinto R, Caniglia M, Lanino E, Messina C, Cesaro S, Letizia C, Bianchini G, Fryssira H, Grabowski P, Shaw N, Bishop N,

- Hughes D, Kapur RP, Datta HK, Taranta A, Fornari R, Migliaccio S, Teti A (2006) Clinical, genetic, and cellular analysis of 49 osteopetrotic patients: implications for diagnosis and treatment. *J Med Genet* 43(4):315–325. doi:[10.1136/jmg.2005.036673](https://doi.org/10.1136/jmg.2005.036673)
31. Pang Q, Chi Y, Zhao Z, Xing X, Li M, Wang O, Jiang Y, Liao R, Sun Y, Dong J, Xia W (2016) Novel mutations of CLCN7 cause autosomal dominant osteopetrosis type II (ADO-II) and intermediate autosomal recessive osteopetrosis (IARO) in Chinese patients. *Osteoporos Int* 27(3):1047–1055. doi:[10.1007/s00198-015-3320-x](https://doi.org/10.1007/s00198-015-3320-x)
32. Gregson CL, Wheeler L, Hardcastle SA, Appleton LH, Addison KA, Brugmans M, Clark GR, Ward KA, Paggiosi M, Stone M, Thomas J, Agarwal R, Poole KE, McCloskey E, Fraser WD, Williams E, Bullock AN, Davey Smith G, Brown MA, Tobias JH, Duncan EL (2016) Mutations in known monogenic high bone mass loci only explain a small proportion of high bone mass cases. *J Bone Miner Res* 31(3):640–649. doi:[10.1002/jbmr.2706](https://doi.org/10.1002/jbmr.2706)
33. Whyte MP, Chines A, Silva DP Jr, Landt Y, Ladenson JH (1996) Creatine kinase brain isoenzyme (BB-CK) presence in serum distinguishes osteopetroses among the sclerosing bone disorders. *J Bone Miner Res* 11(10):1438–1443. doi:[10.1002/jbmr.5650111010](https://doi.org/10.1002/jbmr.5650111010)
34. Hahn M, Vogel M, Amling M, Ritzel H, Delling G (1995) Microcallus formations of the cancellous bone: a quantitative analysis of the human spine. *J Bone Miner Res* 10(9):1410–1416. doi:[10.1002/jbmr.5650100919](https://doi.org/10.1002/jbmr.5650100919)
35. Busse B, Bale HA, Zimmermann EA, Panganiban B, Barth HD, Carriero A, Vettorazzi E, Zustin J, Hahn M, Ager JW 3rd, Puschel K, Amling M, Ritchie RO (2013) Vitamin D deficiency induces early signs of aging in human bone, increasing the risk of fracture. *Sci Transl Med* 5(193):188. doi:[10.1126/scitranslmed.3006286](https://doi.org/10.1126/scitranslmed.3006286)
36. Everts V, de Vries TJ, Helfrich MH (2009) Osteoclast heterogeneity: lessons from osteopetrosis and inflammatory conditions. *Biochim Biophys Acta* 1792(8):757–765. doi:[10.1016/j.bbadis.2009.05.004](https://doi.org/10.1016/j.bbadis.2009.05.004)
37. Neutzsky-Wulff AV, Sims NA, Supanchart C, Kornak U, Felsenberg D, Poulton IJ, Martin TJ, Karsdal MA, Henriksen K (2010) Severe developmental bone phenotype in CLC-7 deficient mice. *Dev Biol* 344(2):1001–1010. doi:[10.1016/j.ydbio.2010.06.018](https://doi.org/10.1016/j.ydbio.2010.06.018)
38. Neutzsky-Wulff AV, Karsdal MA, Henriksen K (2008) Characterization of the bone phenotype in CLC-7-deficient mice. *Calcif Tissue Int* 83(6):425–437. doi:[10.1007/s00223-008-9185-7](https://doi.org/10.1007/s00223-008-9185-7)
39. Roschger P, Paschalis EP, Fratzl P, Klaushofer K (2008) Bone mineralization density distribution in health and disease. *Bone* 42(3):456–466. doi:[10.1016/j.bone.2007.10.021](https://doi.org/10.1016/j.bone.2007.10.021)